scientific reports

Check for updates

OPEN

Automated OCT-tailored and same-visit biomarker-targeted microperimetry in geographic atrophy

Merle Tratnig-Frankl[1,2], Lukas Kuchernig[2], Klaudia Birner[1,2], Simon Schürer-Waldheim[1], Anna Eidenberger[1,2], Johannes Schrittwieser[1,2], Markus Gumpinger[1], Georg Faustmann[1], Magdalena Baratsits[2], Oliver Leingang[3], Gregor S. Reiter[1,2] & Ursula Schmidt-Erfurth[1]✉

This proof-of-concept study developed and validated an automated, biomarker-targeted, real-time microperimetry (MP) approach for individualized structure-function assessment in geographic atrophy (GA). Patients underwent volumetric spectral-domain optical coherence tomography (OCT) and mesopic MP. Automated deep learning-based OCT segmentation using a clinically validated software was applied to identify regions of ellipsoid zone loss (EZL) and retinal pigment epithelium loss (RPEL). A rule-based algorithm then selected 40 biomarker-targeted retinal test locations, with test-point density dynamically adapted to individual lesion morphology and deliberately prioritized within EZL rather than uniformly distributed. Statistical analysis employed multivariable mixed-effects models. In 64 eyes from 44 patients (mean age 79.1 ± 5.0 years; 59% female), 2,560 targeted MP stimuli were tested. Mean retinal sensitivity (RS) was 7.2 ± 7.4 dB in RPEL, 13.3 ± 7.1 dB in EZL, and 19.0 ± 5.0 dB in preserved retina ($p < 0.001$). The median deviation between intended and actual test locations was 38.2 µm (IQR 24.6–59.3 µm), with 98.5% of points correctly localized. This OCT-based, biomarker-guided MP approach enables precise, patient-specific structure-function mapping within a single visit and may serve as a sensitive functional endpoint in future GA trials and clinical practice.

Geographic atrophy (GA), a late-stage form of age-related macular degeneration (AMD), is a major cause of irreversible vision loss in the elderly. This condition is characterized by progressive degeneration of the retinal pigment epithelium (RPE) and the outer photoreceptor layer/ellipsoid zone (EZ), accompanied by alterations in the choriocapillaris, gliosis, synaptic remodelling, and deposition of basal laminar material[1]. Novel FDA (U.S. Food and Drug Administration)-approved therapies, pegcetacoplan and avacincaptad pegol, have demonstrated evidence to slow the morphological/structural progression of GA significantly, underscoring a pivotal advancement in therapeutic intervention. The FDA currently accepts change in GA lesion area measured by fundus autofluorescence (FAF) as the primary structural endpoint for clinical trials. Both agents significantly slowed GA lesion growth based on this FAF-derived structural endpoint in the clinical phase III trials compared to sham, leading to regulatory approval[2,3]. In parallel, OCT-based biomarkers such as RPE and EZ integrity have emerged as key indicators of disease progression in GA. These OCT-derived biomarkers extend beyond the FDA-accepted FAF endpoint by providing high-resolution, layer-specific assessment of retinal degeneration. While FAF primarily functions as a binary grading system for RPE atrophy presence or absence, OCT enables detailed quantification of both RPE loss (RPEL) and photoreceptor/ EZ degeneration, with automated OCT measurements of RPEL showing high correlation to manual FAF-based GA measurements[4]. Importantly, EZ loss (EZL) on OCT is generally larger than areas of RPEL, supporting the hypothesis that photoreceptor degeneration exceeds underlying RPEL as a fundamental pathophysiology in GA progression[5,6]. AI-based 3D OCT segmentation enables reproducible, high-resolution biomarker analysis for detailed assessment, offering potential as complementary or alternative endpoints that more comprehensively capture disease activity and therapeutic response.

While structural endpoints have demonstrated treatment effects, proving corresponding functional benefit remains difficult. In 2024, the European Medicines Agency (EMA) rejected pegcetacoplan's approval referring

[1]Laboratory of Ophthalmic Image Analysis, Medical University of Vienna, Center for Cancer Research (CCR), Vienna, Austria. [2]Department of Ophthalmology and Optometry, Medical University of Vienna, Vienna, Austria. [3]RetInSight GmbH, Vienna, Austria. ✉email: ursula.schmidt-erfurth@meduniwien.ac.at

to a lack of functional evidence, as BCVA outcomes in OAKS and DERBY showed no significant difference at 24 months[7]. This has sparked discussions about suitable functional study endpoints for GA trials. BCVA and low-luminance visual acuity LLVA often remain stable until late disease stages and fail to reflect individual visual dysfunction[8–10]. Other measures like contrast sensitivity and reading speed are more patient-relevant but still fovea-centric[11]. Microperimetry (MP) offers a more sensitive alternative by mapping macular retinal sensitivity (RS), enabling detection of localized deficits[12]. Post-hoc analyses have correlated RS with structural features by AI-based superimposition of MP test points onto OCT data[13,14].

Despite its potential, conventional MP employing predefined, device-specific stimulus grids with fixed test point locations applied uniformly across patients, independent of individual retinal pathology faces strong limitations when applied to patients with GA. Most test points are lost to locations within absolute scotoma over the lesion area affected by complete RPEL and EZL or within intact retina surrounding the lesion reducing the test's informativeness.

Prior studies have demonstrated robust structure-function relationships in GA using retrospective post-hoc analyses, in which MP data are superimposed onto OCT-defined lesions after testing[15–17]. However, these approaches remain limited by their retrospective nature and thus cannot prospectively target areas of interest, i.e. areas of disease activity with progressive sensitivity loss. More recent work has introduced prospective MP strategies informed by structural information, including lesion-adapted grids and standardised spatial concepts based on areas of early atrophy or fixed distances from unifocal atrophy margins[18,19]. These approaches represent a substantial methodological advance beyond uniform fixed grids in GA. High-density MP designs, as demonstrated by Wu et al., have further enabled detailed characterization of early functional changes. However, these were confined to a small region and only for unifocal GA but thus provided important mechanistic insights on early GA as a focal event[20,21]. However, these strategies are not designed to dynamically target early functional deficits, e.g. within photoreceptor degeneration or to scale across larger, morphologically complex, or multifocal GA. In contrast, our study prospectively integrates OCT-derived biomarkers to generate individualized MP patterns that explicitly prioritize EZL as a marker of active disease involvement, enabling lesion-adaptive functional assessment within a single visit.

AI-assisted post-hoc analyses enable the correlation of reduced sensitivity with morphological disruptions in the EZ and thinning of the RPE, thus bridging the gap between functional and structural assessments[22]. Our group has demonstrated that in GA due to AMD, morphological progression is driven by primary EZL subsequently followed by RPEL[23]. Area and location of EZ loss are highly variable between individual GA lesions. Automated deep learning-based layer segmentation of OCT volumes using the certified GA Monitor (RetInSight, Vienna, Austria) enables identification and visualization EZL and RPEL, representing areas of progressive photoreceptor alteration and based on pixel-wise thickness measurements, thereby allowing biomarker-driven functional testing[22]. In this proof-of-concept study, we present an individualized, automated MP strategy that prospectively incorporates real-time OCT biomarker segmentation to guide efficient test point placement. Specifically, we target regions of EZL and RPEL, following the concept that EZL reflects photoreceptor dysfunction and precedes lesion expansion[24].

Our aim was to integrate advanced imaging of GA with MP to generate a biomarker-driven, high-resolution structure-function map. This approach improves spatial precision compared to conventional MP and builds on prior studies suggesting that EZL areas are linked to sensitivity loss and GA progression[25–27]. Specifically, we sought to (1) validate customized MP patterns for GA-specific functional changes, (2) correlate MP sensitivity with OCT-defined EZL and RPEL, and (3) assess the relevance of these correlations for clinical endpoints in GA.

Methods

Patient cohort

Participants aged 55 years and older were enrolled at the Department of Ophthalmology and Optometry, Medical University of Vienna, Austria. Prior to participation, all individuals provided written informed consent in accordance with the Declaration of Helsinki. The study received approval from the institutional independent ethics committee (Medical University of Vienna, reference number 569/2011). All methods were performed in accordance with the relevant guidelines and regulations.

Inclusion criteria comprised both extrafoveal and subfoveal GA, confirmed by OCT imaging. Eyes in which GA extended beyond the OCT scan area were excluded, while lesions abutting the scan border were tolerated. The diagnosis of complete RPE and outer retinal atrophy (cRORA) was based on the CAM consensus criteria, which require a continuous area of RPE loss exceeding 250 µm in diameter, associated choroidal hypertransmission of at least 250 µm, and overlying photoreceptor degeneration, in the absence of RPE tears[28]. Participants with co-existent ocular disease affecting retinal structure or function were excluded, including advanced glaucoma, high myopia (> -6 dpt), significant cataract, recent major ocular surgery, known retinal toxicity from medication (e.g. hydroxychloroquine, tamoxifen), macular atrophy attributable to non-AMD causes, signs of macular neovascularization on OCT angiography (OCTA), or a history of anti-VEGF therapy.

Imaging and lesion-tailored microperimetry protocol

Figure 1 shows a schematic illustration of the workflow with all required steps to create the individual MP pattern. The cohort was imaged using a Spectralis device (Heidelberg Engineering, Heidelberg, Germany) with 512 A-scans per 193 B-scans covering a $20 \times 20°$ macular cube. Images were foveally centred with manual identification of the fovea and corrected if needed prior to image acquisition. During the baseline visit, patients underwent two rounds of MP testing following pupillary dilation with 0.5% Tropicamide. Testing was performed using the Macular Integrity Assessment (MAIA) device (CenterVue S.p.A. (iCare), Padova, Italy) under mesopic standard conditions (4 asb, 1.27 cd/m^2). A 4 – 2 staircase stimulation strategy was applied, with the initial stimulus set at 17 dB. Sensitivity was measured within a range of 0–36 dB. All stimulus points were presented with a

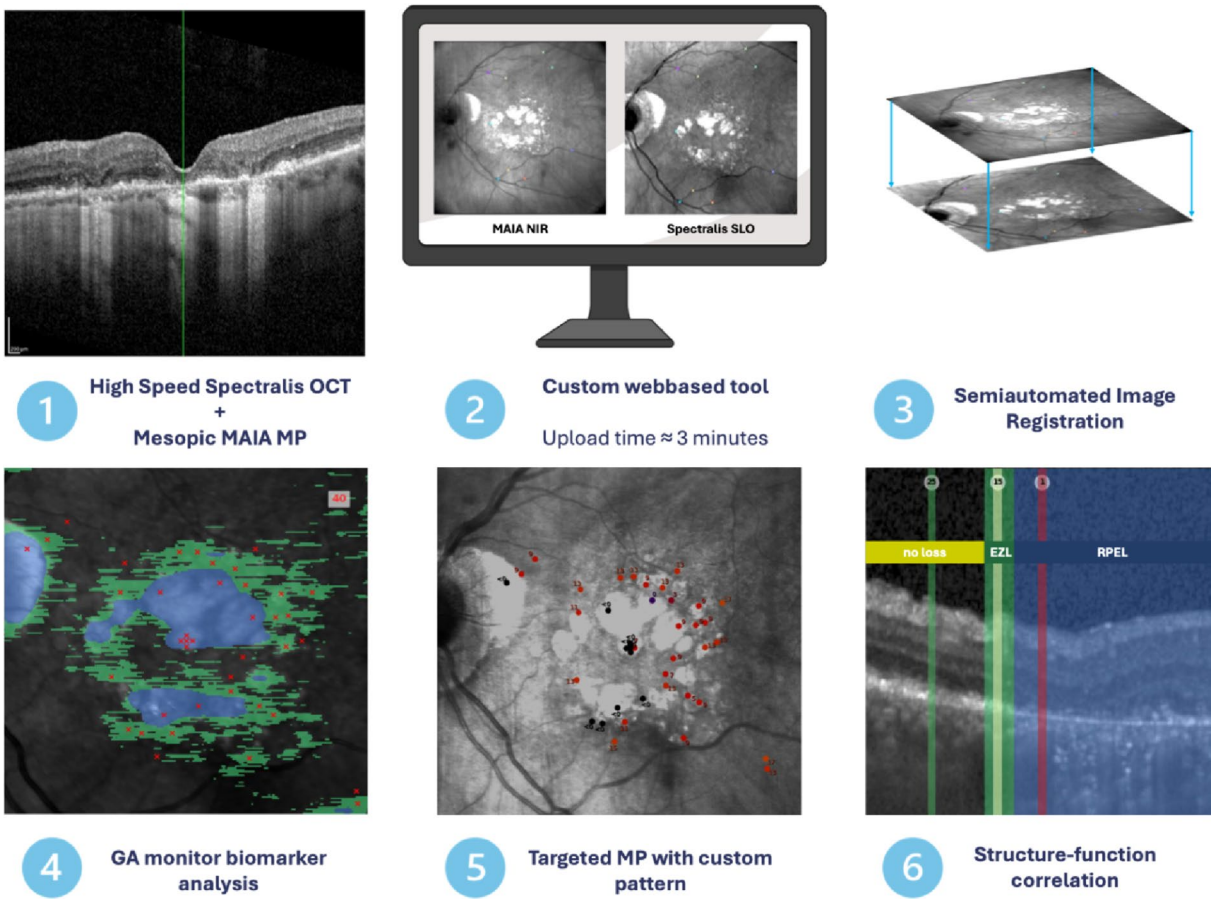

Fig. 1. Automated detection and real-time registration of biomarker-targeted test points using OCT-based segmentation. Schematic illustration of the proposed framework for targeted RS testing in GA in a single study eye. (1) OCT B-Scan (Spectralis HRA + OCT, High Speed, 20° x 20°, 193 B-scans) and a standard four-point MP pattern is tested. (2) Custom-built web-based tool to upload MP and OCT. (3) Semiautomated image registration allowing for OCT coordinates to be superimposed onto the MAIA NIR. (4) OCT volumes were segmented to identify RPEL and EZL using the GA Monitor. (5) A novel targeting algorithm enabling testing at structurally defined regions. (6) with subsequent structure-function correlation, correlating anatomical biomarkers with functional RS.

standard Goldmann III stimulus size and a duration of 200 ms with a standard fixation targeted of a 1° red circle, with a luminance of approximately 10 ± 3 apostilbs. Initially, patients underwent a baseline examination using a four-point balanced pattern test on the MAIA device. This step was used to acquire the near-infrared reflectance fundus image required for registration of the OCT-defined test locations and served as a short familiarisation phase for the patient. The pattern itself was random and the measurements were not included in the functional analysis. In the second round of MP, a lesion-specific pattern with 40 test points was assessed (Fig. 1). The number of test locations was chosen to balance spatial sampling with clinical feasibility, as the targeted approach focuses on OCT-defined regions of interest rather than dense macular sampling. Test reliability was assessed during acquisition using standard MAIA reliability outputs and expert review. No examinations were excluded due to unreliable response behaviour.

Registration and AI-based biomarker analysis

Following acquisition of Spectralis OCT and a four-point MAIA MP, both datasets were manually exported from the two devices and uploaded to a custom-built, web-based tool developed in-house. OCT volumes were automatically segmented using the GA Monitor v2.0 (RetInSight, Vienna, Austria), enabling visualization and quantification of regions of EZL and RPEL, which were subsequently used to guide targeted MP testing. The GA Monitor is a validated, MDR-approved (Medical Device Regulation) segmentation tool for OCT-based GA analysis, described in detail and evaluated in previous studies. [5] Its performance has been independently assessed, demonstrating high reliability across different readers and imaging conditions. All segmentation outputs were visually reviewed for plausibility, including in challenging regions such as lesion borders and areas with heterogeneous signal characteristics. No manual corrections were applied, and cases with gross segmentation errors would have been excluded, to preserve a fully automated, objective, and clinically scalable workflow (Table 1).

Biomarker region	EZ thickness	RPE thickness	Interpretation
Outside Loss (OL)	> 0	> 0	No EZ or RPE loss*
EZ loss (EZL)	= 0	> 0	EZ loss with preserved RPE
RPE loss (RPEL)	= 0	= 0	Atrophy with combined EZ and RPE loss

Table 1. Rule-based definition of OCT-derived biomarker regions. Thickness is measured pixel-wise; values of 0 correspond to thickness < 3.9 µm. *may include other layer pathologies and EZ thinning.

Subsequently, a fully automated custom software pipeline developed in Python 3.8.0 (Python Software Foundation, Wilmington, United States) was employed to allocate 40 test points across three predefined structural regions: EZL, RPEL, and areas without detectable outer retinal loss ("outside loss"), as described below. To enable spatial alignment of structure and function, the MAIA near-infrared reflectance (NIR) image was semi-automatically co-registered with the Spectralis NIR image. Registration was achieved through landmark-based alignment of corresponding vascular features visible in both modalities, manually performed by expert readers trained according to standardised reading-centre operating procedures, including predefined landmark selection and expert visual quality control. Since Spectralis NIR and OCT B-scans are intrinsically co-registered by the device software, this enabled transfer of biomarker-based spatial information to the MAIA system. The resulting individual, OCT-guided MP pattern was then manually imported to the MAIA device. A new exam back up with now 40 custom points replaced the original baseline exam file, allowing the use of the MAIA follow up function, which reportedly allows precise retinal realignment with minor deviations reported by the manufacturer[29]. The upload to the web-based tool, including GA Monitor layer segmentation and MP point distribution, takes two to five minutes. The generation of the individualized MP pattern was performed within a single patient visit.

Lesion-tailored MP pattern software

As shown in Fig. 2, customized MP grids were generated using a rule-based automated point distribution algorithm informed by OCT-based biomarker maps (EZL, RPEL, OL). Each grid was initiated with five foveal control points at the presumed foveal centre of the OCT volume, aligned with the default fovea-centred positioning of the Spectralis system. Test locations within EZL were deliberately prioritized, with test-point density dynamically adapted to individual lesion morphology rather than uniformly distributed across biomarker regions. To account for potential spatial inaccuracies arising from OCT-fundus image registration and minor deviations during MAIA follow-up tracking, predefined safety margins were introduced to ensure that test points remained within the intended biomarker regions (≥ 100 µm from adjacent OL or RPEL, ≥ 200 µm from RPEL for control points). Further, we introduced a minimum spacing requirements (≥ 150 µm between EZL points, ≥ 200 µm between control points) to minimize boundary effects. To further manage variability near lesion borders, biomarker boundary regions were excluded prior to point allocation to maintain safety margins around the test points. 35 individual test points were allocated per eye, including six EZL anchor points with paired control points in OL and/or RPEL where feasible, and additional EZL points distributed to ensure coverage across eccentricities. If the available EZL area was insufficient after erosion and spacing constraints, points were reallocated to OL or RPEL according to predefined fallback rules. A detailed description of the rule-based algorithm is provided in the supplements.

Post-hoc image analysis

To evaluate whether biomarker-based stimulus placement enhances the RS assessment and specificity of functional assessments in GA, a post-hoc comparison of RS across three predefined OCT-derived anatomical biomarkers was performed: areas with complete RPEL, areas with EZL, and areas without detectable outer retinal damage (OL). The biomarker quantifications and en-face map used were derived from automated segmentations as an integral part of the RetInSight GA Monitor software, based on OCT imaging. A 70 µm radius around the stimulus point was used for biomarker analysis of RPEL, EZL and EZ thickness, approximating to the Goldmann III stimulus size of 0.43° (approx. 124 µm in emmetropic eyes), while allowing a small buffer for potential spatial uncertainties, optical blur, and light scatter of the stimulus. EZ thickness was defined as the distance between the inner boundary ellipsoid zone and the outer boundary interdigitation zone (i.e., the third hyperreflective outer retinal band). [27] EZ and RPE loss were segmented using an ensemble of four U-shaped CNNs, with EZ loss defined as ≤ 3,98 µm thickness (one pixel). If no upper layer could be defined, an absence of EZ and thus a thickness of 0 was assumed. Foveal sparing and centre point involvement was manually graded on OCT by expert readers.

Statistical analysis

Descriptive statistics were reported as means ± SD for normally distributed and medians with IQR for skewed data. A pointwise multivariable linear mixed-effects model assessed RS across structural zones (outside loss, EZL, RPEL), with eccentricity, age, gender, and EZ thickness as fixed effects, and patient ID as a random effect. At the eye level, three multivariable models were computed: (1) a composite model with EZL and RPEL, (2) EZL only, and (3) RPEL only, all adjusted for age and eccentricity. Due to collinearity ($r = 0.89$), separate models were used to disentangle effects. Square-root transformed EZL and RPEL were tested in a secondary composite model to account for lesion size non-linearity. Collinearity among predictors was evaluated using Pearson correlation coefficients and variance inflation factors (VIF). High collinearity (VIFs > 5) between EZL and RPEL area was

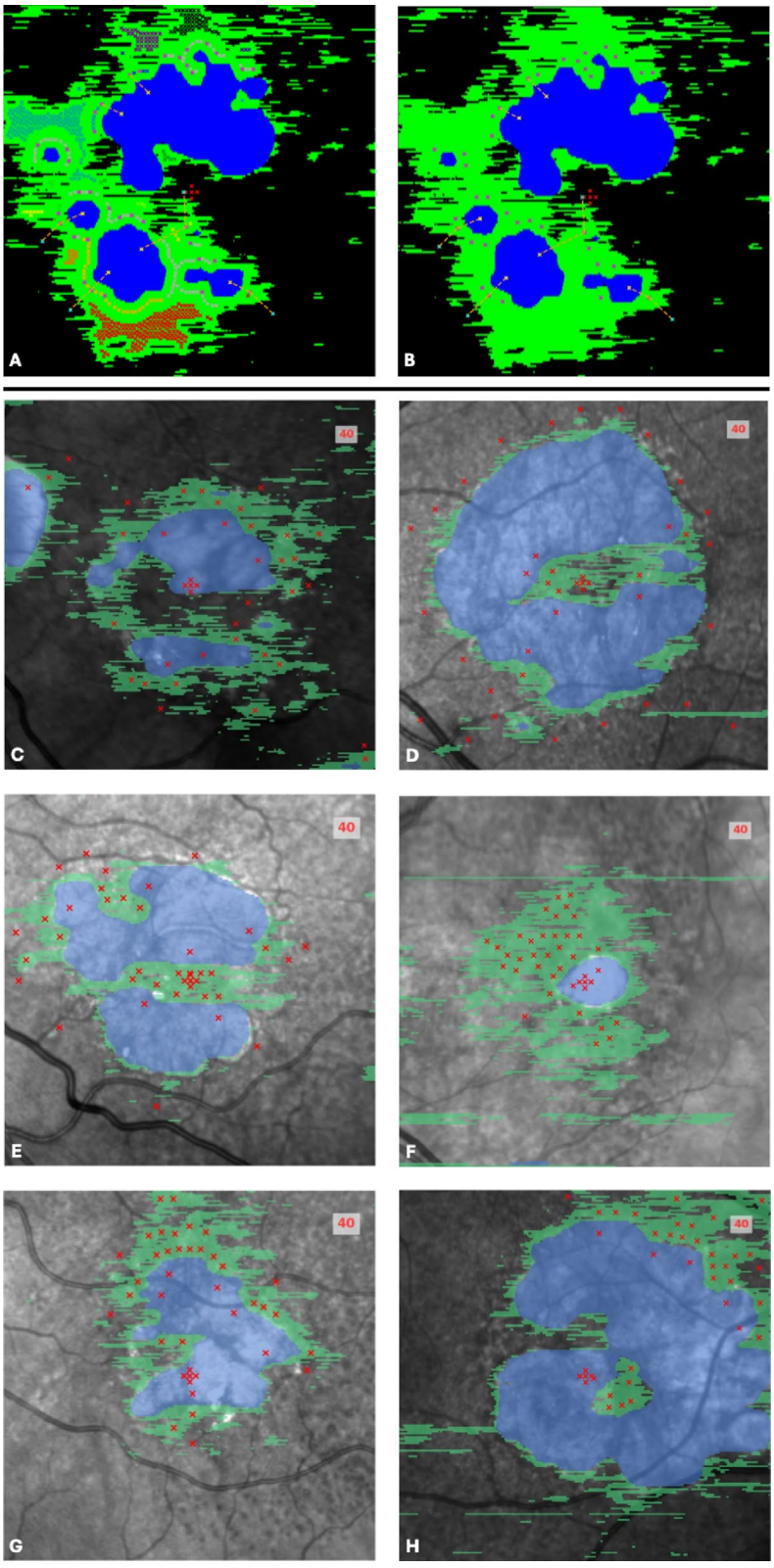

Fig. 2. Custom software distributing MP points within defined OCT biomarkers. En face GA Monitor map based on Spectralis OCT layer segmentation, EZL=green, RPEL=blue. Image (**A**) shows multi-coloured crosses representing all points identified within the EZL as clusters (each EZL cluster is shown in a different colour), which maintain the required safety margins of 100 µm to adjacent area borders. Five red crosses in the image centre represent foveal points, standardised in all MP patterns. Image (**B**) shows all 40 chosen MP points within the EZL (pink) area with control points within RPEL (yellow) and outside loss (turquoise). Images C-H show six characteristic examples of individual OCT en face analysis using the GA monitor and the identified MP test points (red crosses) using the novel algorithm.

addressed by fitting separate models to explore their individual effects on RS, whereas eccentricity showed low collinearity with biomarker category. Random-intercept models were used to account for within-patient clustering. Random slopes were explored but not retained due to lack of improvement in model fit. All models converged within 14–15 iterations, residuals were approximately normal. A separate model assessed RS-BCVA associations using a random intercept for patient ID. Global or foveal RS (points 1–5) served as predictors, adjusted for age and gender. Predicted BCVA values were visualized using ggplot2, holding covariates at cohort medians. All statistical analyses were performed using R (R Foundation for Statistical Computing, Vienna, Austria) within the RStudio environment, with mixed-effects models fitted using the lme4 package.

Results

Cohort characteristics

OCT biomarker-targeted, lesion-specific MP test grids were generated and evaluated in 64 eyes from 44 patients with GA. After excluding two eyes due to manual registration errors and one due to a MAIA device malfunction, a total of 61 eyes from 44 patients with a mean age of 79.1 ± 5.03 years remained for analysis. In total, 11,773 B-scans and 2,440 MP test stimuli were collected. Descriptive statistics for the patient cohort and the distribution of test points across OCT biomarkers are summarized in Table 2. All baseline examinations were conducted within a two-month recruitment period (August-September 2024). Mean MP exam duration was 379.13 s (= 6.32 min).

Retinal sensitivity by biomarker area

RS differed significantly by structural features, a boxplot with representative OCT B-scan example is shown in Fig. 3. Points located within intact retina (OL) had the highest mean RS (18.2 ± 4.94 dB), followed by those associated with EZL overlying intact RPE (13.3 ± 7.07 dB), and those within complete RPEL showing the lowest RS (7.4 ± 7.40 dB). A linear mixed-effects model demonstrated a statistically significant effect of the underlying biomarker on RS ($p < 0.001$), with all pairwise comparisons remaining significant after Tukey correction ($p < 0.001$). The model estimated a + 2.69 dB higher sensitivity for points in preserved retina compared to EZL ($p < 0.001$), and a -5.08 dB lower sensitivity in RPEL compared to EZL ($p < 0.001$). All models were adjusted for age, gender, and eccentricity. Only the 35 individually targeted MP points were considered, the five foveal points were excluded for this analysis (Table 3).

Eye-level predictors of mean retinal sensitivity

A multivariable linear mixed-effects model was calculated using eye-level mean RS as the outcome to evaluate the predictive value of global structural biomarkers. Predictors included total EZL and RPEL areas, age, and test point eccentricity (Table 4). EZL was significantly associated with reduced RS (estimate: -0.038 dB/mm², 95% CI: -0.060 to -0.016; $p = 0.001$), while RPEL trended toward significance (-0.013 dB/mm², 95% CI: -0.027 to 0.001; $p = 0.057$). At the eye level, increasing mean test-point eccentricity was associated with lower mean RS (-0.180 dB/°, $p < 0.001$), consistent with physiological eccentricity-related sensitivity decline and distinct from the pointwise structure–function analyses, where local biomarker distribution dominates RS. In the eye-level models, EZL and RPEL areas refer to the total lesion areas within the OCT volume, whereas the pointwise analyses classify the local biomarker status at each stimulus location based on the 70 µm stimulus radius.

Due to the high collinearity between EZL and RPEL (Pearson's $r = 0.89$; VIF > 5), two additional models were calculated including either EZL or RPEL alone (Supplementary Table 4 A-B). Both confirmed a significant

Patient Characteristics	
No. of eyes (R: L)	64 (33:31)
No. of patients (F: M)	44 (26:18)
Age, years, mean ± SD	79.1 ± 5.03
BCVA, ETDRS letters, mean ± SD	64.03 ± 12.01
GA Characteristics	
Mean RPEL area (mm²)	5.10 ± 4.14
Mean EZL area (mm²)	8.86 ± 5.40
Foveal Sparing (%)	
complete (%)	38.1
partial (%)	46.0
Centre Point Involvement (%)	58.7
MP Point Distribution	
RPEL (%)	10.6
EZL (%)	41.0
Outside loss (%)	48.2

Table 2. Cohort Characteristics. Including Patient Cohort, GA characteristics, RPEL and EZL area obtained from the GA monitor, foveal sparing and centre point involvement as graded in Spectralis OCT, MP point distribution in targeted MP.

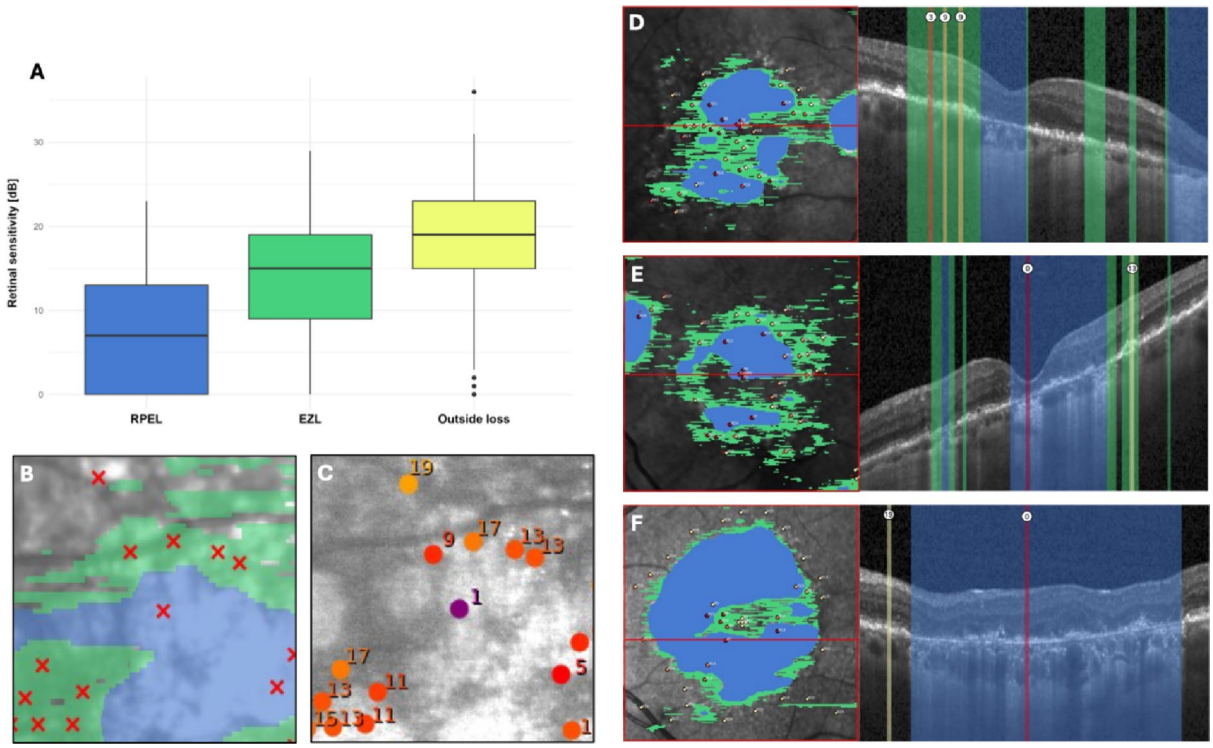

Fig. 3. RS by biomarker zone, (**A**) Boxplots depict the median, interquartile range (IQR), and distribution of RS across three structural zones: RPEL, EZL and preserved retina (outside loss). (**B**) En face GA Monitor image showing identified regions of interest (ROI), with red crosses marking intended MP test locations. (**C**) Corresponding mesopic MP map displaying RS values at each location, colour-coded in dB. (**D**-**F**) OCT en-face and B-scan illustrations: left column shows the en face view indicating the B-scan location shown on the right (red line) and segmented biomarker areas (RPEL = blue, EZL = green) and the individual MP test points (numbered) with colour-coded RS; right column shows the corresponding individual B-scans with MP test points and RS values indicated in circles (in dB).RPEL=blue, EZL=green and RS values colour scale coded.

Predictor	Estimate	Std. Error	95% CI	*p*-value
Intercept	25.42	11.46	[3.06, 47.78]	0.032
Outside Loss	2.69	0.26	[2.18, 3.20]	$<2\times10^{-16}$
RPE Loss	-5.08	0.34	[-5.74, -4.42]	$<2\times10^{-16}$
Age	-0.15	0.14	[-0.41, 0.11]	0.30
Gender (Female)	-0.27	1.42	[-3.05, 2.51]	0.85
Distance to Fovea	0.48	0.15	[0.19, 0.77]	0.0014

Table 3. Multivariable Linear Mixed-Effects Model of Pointwise RS by OCT Biomarker Area. Fixed effects from a multivariable linear mixed-effects model, including patient ID as a random effect. All predictors were simultaneously included. This model analyses test-point-level RS as a function of anatomical feature area (Outside Loss, EZL [reference], RPEL), adjusted for age, gender, and distance from the fovea.

negative association with RS (EZL-only: -0.037 dB/mm², $p=0.001$; RPEL-only: -0.016 dB/mm², $p=0.045$), supporting the individual contribution of each parameter.

To further confirm the robustness of findings, we repeated the analysis using square-root transformed predictors. Results remained consistent (√EZL: −0.480 dB/mm, $p=0.004$; √RPEL: -0.260 dB/mm, $p=0.072$; Supplementary Table 5), supporting the validity of the untransformed model.

Accuracy and reliability of test point location

The accuracy of stimulus placement was evaluated by comparing the intended OCT-derived coordinates with the actual test point locations recorded by the MAIA device, depicted in Fig. 4 (A). The median deviation between intended and actual placement was 38.8 µm (IQR: 24.9–61.5 µm), and 90% of all test points deviated less than 120 µm. These results confirm high spatial precision of the transfer process.

To validate structural-functional mapping, each test point was reclassified post-hoc to confirm its location within the intended biomarker area (Fig. 4B). 98.5% of points matched their assigned zones at the centre point,

Predictor	Estimate	*p*-value	95% CI	*n*
EZL area (mm²)	-0.038	0.001	-0.060 to -0.016	61
RPEL area (mm²)	-0.013	0.057	-0.027 to 0.001	61
Age (years)	-0.015	0.083	-0.033 to 0.003	61
Distance to fovea (°)	-0.18	< 0.001	-0.23 to -0.14	61

Table 4. Eye-level multivariable model including EZL and RPEL to predict mean retinal sensitivity (RS). Multivariable linear mixed-effects model with eye-level mean RS as outcome. Predictors included total EZL and RPEL area, age, and test point eccentricity. High collinearity was observed between EZL and RPEL (Pearson's $r = 0.89$; VIF > 5).

supporting the predefined safety margins (100 µm for EZL and outside loss, 200 µm for RPEL) and minimizing cross-contamination between regions. Figure 4C-F illustrates examples from two patients with low and high MP point deviation with Fig. 4D showing deliberately an extreme example of fundus-OCT registration deviation to illustrate that, even under substantial mis-registration, predefined safety margins largely preserve correct biomarker-targeted test-point allocation. We also assessed whether fixation stability affected test point deviation. While mean deviation varied across stability classes, differences were not statistically significant ($p = 0.070$).

Discussion

Our study introduces proof-of-concept for a novel same-visit approach to targeted MP in GA by integrating OCT biomarker analysis. Unlike conventional fixed MP grids, our method tailors stimulus placement based on EZL and RPEL in one visit, aligning functional testing with structural alteration. Combining automated detection of OCT anatomic biomarkers with targeted functional test point placement enhances the efficacy and objectivity of structure-function correlation in GA. By focusing on EZL areas, decreases in retinal function can be detected before scotoma formation, enabling monitoring of progressive visual loss, including potential impact on patient quality of life as a patient-relevant trial outcome.

Previous studies have demonstrated the potential of MP in assessing functional impairment in macular disease including GA.[19,30] Scientific consensus highlights the correlation between photoreceptor degeneration and declining retinal sensitivity, particularly in regions adjacent to RPE atrophy referred to as the clinical lesion[17]. While informative, these studies often used standardised MP grids or fixed distances around atrophy, which may miss localized functional changes. The test pattern referred to as "onion ring" shape around a 250 µm junctional zone band does not reflect the biological irregularity of disease progression based on a most irregular presence and extension of EZL[23].

Our study builds on our group's previous work on automated OCT-based biomarker analysis[5], Automated structure-function correlation[31], the characterization of EZL as an early structural marker that precedes RPEL in GA[27]. While prior AI-assisted post-hoc analyses successfully linked RS loss to structural biomarkers[13,32], they lacked real-time integration. In contrast, our approach enables an automated prospective test point pattern algorithm for structure-function assessment. A key advantage is the same-visit visualization and quantification of three GA-relevant biomarkers, EZL, RPEL, and intact retina, via a quick fully automated tool accessible to any clinician using Spectralis. The system is MDR-approved in the EU, CH, GB, and Australia; investigational use is possible elsewhere. No specific PACS is required, as direct upload via RETHub (RetInSight, Vienna) is user-friendly and widely compatible.

Our results show significant differences in RS across the three predefined biomarker zones, RPEL, EZL, and preserved retina. EZL regions consistently demonstrate reduced RS compared to RPEL, confirming early functional loss at the level of photoreceptor disruption[33,34]. As EZL loss precedes RPEL loss, targeting EZL enables sensitive detection of functional decline during disease progression. This can enhance GA trial sensitivity, especially compared to BCVA, which often misses to capture early dysfunction[28]. We further show that structure-function relationships are influenced by local context and foveal distance, not just anatomical classification. Even after adjusting for age and eccentricity, EZL and RPEL remained primary functional predictors. Although pointwise analyses may give the impression of higher retinal sensitivity at greater eccentricities due to non-uniform lesion distribution, eye-level modelling confirmed a physiological decline in sensitivity with increasing distance from the fovea, indicating that local functional changes in GA are primarily driven by underlying structural biomarkers rather than eccentricity alone.

Contrary to expectations, RS in RPEL areas was not uniformly 0 dB, suggesting residual function. This may reflect remaining RPE debris[35], adjacent photoreceptor activity[36], light scatter beyond test locations[37], or contributions from the ONL, which corresponds to photoreceptor nuclei and affects RS when thinned[38].

Analysis of point placement deviation showed that safety margins were rarely exceeded, confirming accurate localization of test points within biomarkers of interest. Minor deviations may result from OCT-MAIA registration assuming emmetropia[39], patient fixation instability, or small tracking errors during follow-up mode[40]. The present analysis does not allow the relative contribution of these factors to be separated, and the observed deviations likely reflect their combined effect. Even in rare cases of substantial spatial deviation, the use of predefined safety margins ensured that test points remained within their intended biomarker regions, supporting robustness of the approach under non-ideal alignment conditions. Still, median deviations remained low, supporting high accuracy in both foveal and extrafoveal lesions. Fixation instability had only a modest impact, allowing inclusion of patients with poor fixation in automated workflows. Inclusion of patients with poor fixation is feasible in our automated workflow due to real-time control of test point placement. Unlike

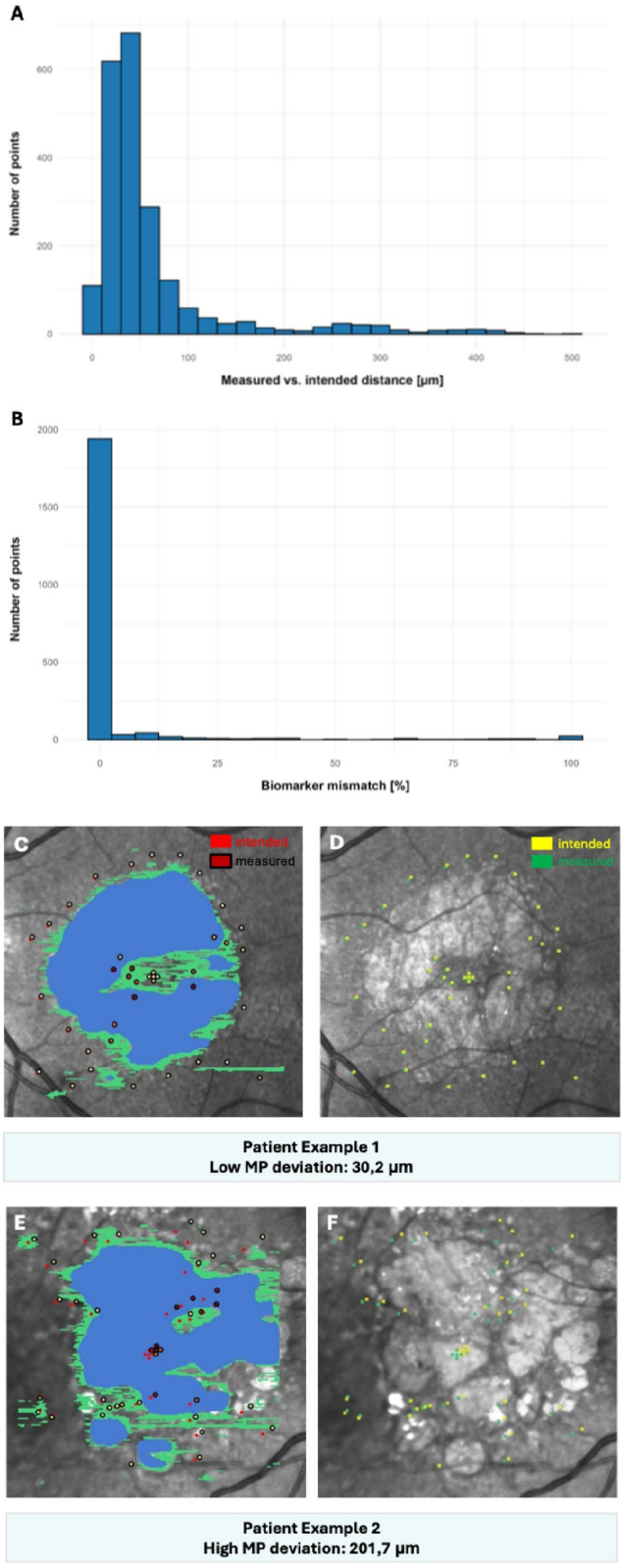

Fig. 4. Accuracy of MP test point placement. (**A**) Histogram of measured versus intended test point deviation measured as distances in µm (**B**) Percentage of MP points matching its designated biomarker zone at the stimulus centre point. (**C**-**F**) Patient example OCT en-face images with individual MP test point map for varying MP point deviation. Images C-D: Patient example 1 with low MP deviation with a mean of 30.2 µm. Images E-F: Patient example 2 with a high MP deviation with a mean of 201.7 µm.

retrospective methods, the operator can monitor and adjust placement accuracy, ensuring reliability. The limited number of 40 test points allows for shorter testing (mean 4–5 min), improving usability in trials and clinical routine.

Large GA trials like OAKS and DERBY enrolled over 2,500 patients over 24 months[2]. While our study was not powered to address sample-size implications, future variance-based simulations may determine whether individualized, biomarker-targeted MP can reduce RS variability and thus support more efficient trial designs[41]. Focusing on regions like EZL, most susceptible to early functional loss, minimizes inter-individual variability and enhances statistical power, possibly facilitating smaller, more efficient trials[22,41]. In a longitudinal setting, maintaining stable individualized test grids across visits while repeatedly updating OCT-based biomarker maps allows functional change to be tracked at identical retinal locations as GA lesions expand. This enables differentiation between true functional decline within a given tissue state and functional loss attributable to anatomical conversion (e.g., EZL to RPEL), without redefining test locations. If reduced variability is confirmed in longitudinal analyses, this targeted strategy has the potential to improve endpoint sensitivity, enable earlier detection of intervention-related effects, and support more statistically efficient trial designs, potentially reducing required sample sizes. This is particularly relevant for GA trials, where slow progression and high functional variability have historically limited the ability to detect treatment effects using conventional endpoints.

In contrast to BCVA, MP captures spatially resolved deficits across the central field, often preceding central vision loss[42]. The strong structure–function alignment of targeted MP underscores its value in clinical trials. These results support growing consensus and EMA guidance, that MP might add critical information, opposed to using just BCVA as a primary functional endpoint in GA trials[43].

While prior research has established AI-based structure-function correlations[32], our approach applies these findings in same-visit clinical assessments, offering immediate insights into disease progression. By integrating AI-based OCT segmentation using an MDR-approved tool, we aimed to facilitate rapid and objective analysis of relevant biomarkers. The combination of the clinically approved GA Monitor, the upcoming MAIA3 MP, a PACS-independent upload tool, RETHub, and custom software enabled real-time structure-function alignment, suggesting that individualized MP may be feasible even in larger clinical settings. Ongoing longitudinal studies will determine whether early functional deficits detected in EZL regions predict subsequent GA progression. By continuously monitoring visual function within the personalized MP grids, we anticipate detecting early RS changes that precede structural GA enlargement. This methodology, if developed further, may improve outcome measures in clinical trials, offering a sensitive tool to assess neuroprotection or disease modification in GA studies.

Disease severity, lesion size, and lesion configuration determine how much structurally informative retina is available for functional testing in GA. A key advantage of the proposed framework is that individualized test-point allocation is driven by OCT-defined lesion morphology and can therefore be applied across unifocal, multifocal, and irregular GA patterns. The approach is particularly informative in eyes with high EZL to RPEL ratio, where functional change is most dynamic. In cases with limited or absent EZL, test points are adaptively reallocated to adjacent intact retina, whereas in advanced GA the algorithm limits oversampling of RPEL, avoiding dominance of absolute scotoma seen with fixed grids. The method reaches its limitation when GA size exceeds OCT volume borders and might falsely place MP test points in areas of peripapillary atrophy, but remains applicable across a broad spectrum of macular GA phenotypes. Limitations include the small sample size, cross-sectional design, and single-centre setting, limiting generalizability and precluding longitudinal conclusions. Test-retest repeatability (ICC/CoR) MP has yet to be analysed to allow separation of fatigue and learning from true effects. However, all participants were MP-naïve and underwent only a brief, standardised familiarization phase, minimizing potential learning effects. Nonetheless, standardised segmentation and automated test grid generation support reproducibility. Multicollinearity between EZL and RPEL complicates regression interpretation, though both were retained for their distinct clinical relevance. Multi-centre longitudinal studies are needed to validate and extend these findings.

Conclusion

This study demonstrates the feasibility of integrating OCT-derived biomarkers into individualized MP testing for GA within a single visit. By prospectively aligning functional assessment with structural alterations, this approach enables pointwise structure–function mapping and highlights the functional relevance of EZL as an early marker of disease involvement. While confirmatory longitudinal studies are required, these findings support the potential of biomarker-guided MP to complement conventional endpoints and inform future clinical trial design as well as clinical practice.

Data availability

The datasets generated and/or analyzed during the current study are available from the corresponding author upon reasonable request. Processed data supporting the findings of this study are available within the article and its supplementary files. OCT biomarker segmentations were generated using the CE-marked GA Monitor software (RetInSight GmbH, Vienna, Austria). Due to patient privacy regulations and data protection laws, raw imaging data cannot be publicly shared but can be made available to qualified researchers under a data-sharing agreement.

Received: 9 October 2025; Accepted: 17 March 2026
Published online: 27 March 2026

References

1. Kinnunen, K., Petrovski, G., Moe, M. C., Berta, A. & Kaarniranta, K. Molecular mechanisms of retinal pigment epithelium damage and development of age-related macular degeneration. *Acta Ophthalmol.* **90** (4), 299–309. https://doi.org/10.1111/j.1755-3768.2011.02179.x (2012).
2. Heier, J. S. et al. Pegcetacoplan for the treatment of geographic atrophy secondary to age-related macular degeneration (OAKS and DERBY): two multicentre, randomised, double-masked, sham-controlled, phase 3 trials. *Lancet* **402** (10411), 1434–1448. https://doi.org/10.1016/S0140-6736(23)01520-9 (2023).
3. Jaffe, G. J. et al. C5 Inhibitor Avacincaptad Pegol for Geographic Atrophy Due to Age-Related Macular Degeneration: A Randomized Pivotal Phase 2/3 Trial. *Ophthalmology* **128** (4), 576–586. https://doi.org/10.1016/j.ophtha.2020.08.027 (2021).
4. Mai, J. et al. Quantitative comparison of automated OCT and conventional FAF-based geographic atrophy measurements in the phase 3 OAKS/DERBY trials. *Sci. Rep.* **14** (1), 20531. https://doi.org/10.1038/s41598-024-71496-y (2024).
5. Mai, J. et al. Clinical validation for automated geographic atrophy monitoring on OCT under complement inhibitory treatment. *Sci. Rep.* **13** (1), 7028. https://doi.org/10.1038/s41598-023-34139-2 (2023).
6. Reiter, G. S. et al. AI in the clinical management of GA: A novel therapeutic universe requires novel tools. *Prog Retin Eye Res.* **103**, 101305. https://doi.org/10.1016/j.preteyeres.2024.101305 (2024).
7. European Medicines Agency. Syfovre (pegcetacoplan). https://www.ema.europa.eu/en/medicines/human/EPAR/syfovre
8. Sunness, J. S. et al. Low luminance visual dysfunction as a predictor of subsequent visual acuity loss from geographic atrophy in age-related macular degeneration. *Ophthalmology* **115** (9), 1480–1488. https://doi.org/10.1016/j.ophtha.2008.03.009 (2008).
9. Pondorfer, S. G. et al. Association of Vision-related Quality of Life with Visual Function in Age-Related Macular Degeneration. *Sci. Rep.* **9** (1), 15326. https://doi.org/10.1038/s41598-019-51769-7 (2019).
10. Sadda, S. R. et al. Clinical endpoints for the study of geographic atrophy secondary to age-related macular degeneration. *Retina* **36** (10), 1806–1822. https://doi.org/10.1097/IAE.0000000000001283 (2016).
11. Varma, R. et al. Maximum Reading Speed in Patients With Geographic Atrophy Secondary to Age-Related Macular Degeneration. *Invest. Ophthalmol. Vis. Sci.* **59** (4), AMD195–AMD201. https://doi.org/10.1167/iovs.18-24238 (2018).
12. Yang, Y. & Dunbar, H. Clinical Perspectives and Trends: Microperimetry as a Trial Endpoint in Retinal Disease. *Ophthalmologica* **244** (5), 418–450. https://doi.org/10.1159/000515148 (2021).
13. Pfau, M. et al. Determinants of Cone and Rod Functions in Geographic Atrophy: AI-Based Structure-Function Correlation. *Am. J. Ophthalmol.* **217**, 162–173. https://doi.org/10.1016/j.ajo.2020.04.003 (2020).
14. Pilotto, E. et al. Microperimetry Features of Geographic Atrophy Identified With En Face Optical Coherence Tomography. *JAMA Ophthalmol.* **134** (8), 873–879. https://doi.org/10.1001/jamaophthalmol.2016.1535 (2016).
15. Saeed, A. et al. Local OCT Structural Correlates of Deep Visual Sensitivity Defects in Early Atrophic Age-Related Macular Degeneration. *Ophthalmol. Retina*. **9** (5), 412–420. https://doi.org/10.1016/j.oret.2024.12.007 (2025).
16. Birner, K. et al. Structure-Function Correlation of Deep-Learning Quantified Ellipsoid Zone and Retinal Pigment Epithelium Loss and Microperimetry in Geographic Atrophy. *Invest. Ophthalmol. Vis. Sci.* **66** (3), 26. https://doi.org/10.1167/iovs.66.3.26 (2025).
17. Meleth, A. D. et al. Changes in retinal sensitivity in geographic atrophy progression as measured by microperimetry. *Invest. Ophthalmol. Vis. Sci.* **52** (2), 1119–1126. https://doi.org/10.1167/iovs.10-6075 (2011).
18. Chang, D. S. et al. Macular Sensitivity Endpoints in Geographic Atrophy: Exploratory Analysis of Chroma and Spectri Clinical Trials. *Ophthalmol. Sci.* **4** (1), 100351. https://doi.org/10.1016/j.xops.2023.100351 (2024).
19. Pfau, M. et al. Mesopic and dark-adapted two-color fundus-controlled perimetry in geographic atrophy secondary to age-related macular degeneration. *Retina* **40** (1), 169–180. https://doi.org/10.1097/IAE.0000000000002337 (2020).
20. Wu, Z. et al. Visual Sensitivity Loss in Geographic Atrophy: Structure-Function Evaluation Using Defect-Mapping Microperimetry. *Invest. Ophthalmol. Vis. Sci.* **65** (1), 36. https://doi.org/10.1167/iovs.65.1.36 (2024).
21. Wu, Z., Hodgson, L. A. B. & Guymer, R. H. Targeted High-Density Microperimetry Testing of Nascent Geographic Atrophy in Age-Related Macular Degeneration. *Ophthalmol. Sci.* **4** (2), 100419. https://doi.org/10.1016/j.xops.2023.100419 (2024).
22. Pfau, M. et al. Progression of Photoreceptor Degeneration in Geographic Atrophy Secondary to Age-related Macular Degeneration. *JAMA Ophthalmol.* **138** (10), 1026–1034. https://doi.org/10.1001/jamaophthalmol.2020.2914 (2020).
23. Schmidt-Erfurth, U. et al. Disease Activity and Therapeutic Response to Pegcetacoplan for Geographic Atrophy Identified by Deep Learning-Based Analysis of OCT. *Ophthalmology* **132** (2), 181–193. https://doi.org/10.1016/j.ophtha.2024.08.017 (2025).
24. Reiter, G. S. et al. Subretinal Drusenoid Deposits and Photoreceptor Loss Detecting Global and Local Progression of Geographic Atrophy by SD-OCT Imaging. *Invest. Opthalmology Visual Sci.* **61** (6), 11. https://doi.org/10.1167/iovs.61.6.11 (2020).
25. Coulibaly, L. M., Mohamed, H., Fuchs, P., Schmidt-Erfurth, U. & Reiter, G. S. Inter and intradevice assessment of microperimetry testing in aging eyes. *Sci. Rep.* **14** (1), 1049. https://doi.org/10.1038/s41598-024-51539-0 (2024).
26. Birner, K. et al. Normative prospective data on automatically quantified retinal morphology correlated to retinal function in healthy ageing eyes by two microperimetry devices. *Acta Ophthalmol.* **103** (4), 423–431. https://doi.org/10.1111/aos.17434 (2025).
27. Birner, K. et al. Structure-Function Correlation of Deep-Learning Quantified Ellipsoid Zone and Retinal Pigment Epithelium Loss and Microperimetry in Geographic Atrophy. *Invest. Ophthalmol. Vis. Sci.* **66** (3), 26. https://doi.org/10.1167/iovs.66.3.26 (2025).
28. Sadda, S. R. et al. Consensus Definition for Atrophy Associated with Age-Related Macular Degeneration on OCT. *Ophthalmology* **125** (4), 537–548. https://doi.org/10.1016/j.ophtha.2017.09.028 (2018).
29. iCare, F. & Oy *MAIA2 Operating Manual, Rev. 2.6*. (2023).
30. Wu, Z., Glover, E. K., Gee, E. E., Hodgson, L. A. B. & Guymer, R. H. Functional Evaluation of Retinal Pigment Epithelium and Outer Retinal Atrophy by High-Density Targeted Microperimetry Testing. *Ophthalmol. Sci.* **4** (2), 100425. https://doi.org/10.1016/j.xops.2023.100425 (2024).
31. Birner, K. et al. Topographic and quantitative correlation of structure and function using deep learning in subclinical biomarkers of intermediate age-related macular degeneration. *Sci. Rep.* **14** (1), 28165. https://doi.org/10.1038/s41598-024-72522-9 (2024).
32. Seeböck, P. et al. Linking Function and Structure with ReSensNet: Predicting Retinal Sensitivity from OCT using Deep Learning. *Ophthalmol. Retina*. **6** (6), 501–511. https://doi.org/10.1016/j.oret.2022.01.021 (2022).
33. Heeren, T. F. C. et al. Longitudinal correlation of ellipsoid zone loss and functional loss in teleangiectasia type 2. *Retina* **38** (1), S20–S26. https://doi.org/10.1097/IAE.0000000000001715 (2018).
34. Wu, Z., De Zanet, S., Blair, J. P. M. & Guymer, R. H. Loss of OCT Outer Retinal Bands as Potential Clinical Trial Endpoints in Intermediate Age-Related Macular Degeneration. *Ophthalmol. Sci.* **5** (4), 100769. https://doi.org/10.1016/j.xops.2025.100769 (2025).
35. Sparrrow, R., Hicks, J. & Hamel, D. P. The Retinal Pigment Epithelium in Health and Disease. *Curr. Mol. Med.* **10** (9), 802–823. https://doi.org/10.2174/156652410793937813 (2010).
36. Wu, Z., Glover, E. K., Gee, E. E., Hodgson, L. A. B. & Guymer, R. H. Functional Evaluation of Retinal Pigment Epithelium and Outer Retinal Atrophy by High-Density Targeted Microperimetry Testing. *Ophthalmol. Sci.* **4** (2), 100425. https://doi.org/10.1016/j.xops.2023.100425 (2024).
37. Ávila, F. J. Scattering Improves Temporal Resolution of Vision: A Pilot Study on Brain Activity. *Photonics* **12** (1), 23. https://doi.org/10.3390/photonics12010023 (2024).
38. Saßmannshausen, M. et al. Structure-Function Analysis in Patients With Intermediate Age-Related Macular Degeneration. *Invest. Opthalmology Visual Sci.* **59** (3), 1599. https://doi.org/10.1167/iovs.17-22712 (2018).
39. Coulibaly, L. M., Mohamed, H., Fuchs, P., Schmidt-Erfurth, U. & Reiter, G. S. Inter and intradevice assessment of microperimetry testing in aging eyes. *Sci. Rep.* **14** (1), 1049. https://doi.org/10.1038/s41598-024-51539-0 (2024).

40. Pfau, M. et al. Visual field indices and patterns of visual field deficits in mesopic and dark-adapted two-colour fundus-controlled perimetry in macular diseases. *Br. J. Ophthalmol.* **102** (8), 1054–1059. https://doi.org/10.1136/bjophthalmol-2017-311012 (2018).
41. Saeed, A. et al. Customized Evaluation of Progressive Visual Sensitivity Loss in Geographic Atrophy to Improve the Power of Clinical Trials. *Ophthalmol. Sci.* **5** (4), 100763. https://doi.org/10.1016/j.xops.2025.100763 (2025).
42. Wu, Z., Ayton, L. N., Guymer, R. H. & Luu, C. D. Low-Luminance Visual Acuity and Microperimetry in Age-Related Macular Degeneration. *Ophthalmology* **121** (8), 1612–1619. https://doi.org/10.1016/j.ophtha.2014.02.005 (2014).
43. Csaky, K. G., Miller, J. M. L., Martin, D. F. & Johnson, M. W. Drug Approval for the Treatment of Geographic Atrophy: How We Got Here and Where We Need to Go. *Am. J. Ophthalmol.* **263**, 231–239. https://doi.org/10.1016/j.ajo.2024.02.021 (2024).

Author contributions

U.S.E., G.R., K.B. and M.T.F conceptualized the study. L.K. created the custom algorithm for individual MP patterns. S.S.W. and M.G. provided the technological pipeline to combine MP and OCT. M.T.F. conducted all patient visits and collected the data with the help of A.E. and J.S. M.B. helped recruiting the patients and conducted the study site coordination and technological support with all devices. S.S.W. and O.L. performed data processing and first analysis. L.K. conducted the statistical analysis with M.T.F. M.T.F. drafted the manuscript. G.R., K.B. and S.E. critically revised the manuscript for important intellectual content. All authors read and approved the final submitted version.

Funding

The GA monitor was provided by RetInSight GmbH, Vienna, Austria.

Declarations

Competing interests

O.L. is an employee of RetInSight GmbH (Vienna, Austria), which provided the GA Monitor software used for biomarker segmentation in this study. U.S.-E. and G.R. are or have been scientific advisors to RetInSight GmbH. The company had no role in data analysis, interpretation, or manuscript preparation. All other authors declare no competing interests.

Disclosures

GR: Scientific consultancy for Apellis Pharmaceuticals, Boehringer, Espansione, Nordic Pharma, Roche and research funding by institution: RetInSight. SE: Scientific consultancy for Abbvie, Apellis Pharmaceuticals, Aviceda, Boehringer, Complement Therapeutics, Heidelberg Engineering, Janssen, Kodiak, Novartis, ONL, Roche, Topcon and research funding by institution: Apellis, Genentech, Heidelberg Engineering, Kodiak, Novartis, RetInSight, Roche.

Additional information

Supplementary Information The online version contains supplementary material available at https://doi.org/10.1038/s41598-026-45253-2.

Correspondence and requests for materials should be addressed to U.S.-E.